J Nanostruct 16(3): 3650-3664, Summer 2026

RESEARCH PAPER

Physicochemical and Biological Evaluation of Iron Oxide–Nanocomposites for Tissue Therapeutic Applications

*Manal Malik Saadoon [1], Rand B. Lutfi [2], Ahmed Al-Amery [3,4], Noor M.Saadoon [5]**

[1] *General Directorate of Education in Baghdad, Baghdad, Iraq*

[2] *Department of Physics, College of Education, Al-Iraqia University, Baghdad, Iraq*

[3] *Department of Physiology, College of Medicine, University of Thi-Qar, Iraq*

[4] *Alsharq College of Specialized Technical Sciences, Iraq*

[5] *Centre of Nanotechnology and Advanced Material, University of Technology, Iraq*

ARTICLE INFO

Article History:
Received 15 April 2026
Accepted 22 June 2026
Published 01 July 2026

Keywords:
Composite
Iron oxide nanoparticles
Nano-carrier
Tissue engineering
Wound dressing

ABSTRACT

The use of nanomaterials is rapidly expanding, and new biomedical studies are being conducted now to enhance the utility and effectiveness of traditional and unmodified drug delivery systems as well as common scaffolds for tissue engineering or advanced hydrogel materials for wound healing. Iron oxide nanoparticles are of particular interest because of their particle shape and size variations and because they possess unique physicochemical characteristics (e.g., high surface area per unit volume, porous structures) that render them ideal nanomaterials for use in numerous areas of medicine and biology.

How to cite this article
Saadoon M., Lutfi R., Al-Amery A., M.Saadoon N. Physicochemical and Biological Evaluation of Iron Oxide–Nanocomposites for Tissue Therapeutic Applications. J Nanostruct, 2026; 16(3):3650-3664. DOI: 10.22052/JNS.2026.03.055

INTRODUCTION

The transition from the macro level to the nano level of matter creates an enormous difference in how our world functions. The rapid pace of technological progress in the nanotechnology field has resulted in many great medical achievements [1]. Nanotechnology can be utilized for a variety of biomedical engineering applications, particularly in drug delivery systems that use nanoparticles (NPs) to deliver therapies for cancer [2]. Due to their unique surface characteristics, NPs are an excellent vehicle for developing therapy delivery systems. In addition, NPs interact with biological systems to provide the opportunity for targeted delivery of drugs, therapeutic monitoring, and therapy [1]. Anti-cancer loaded nanoparticles can avoid being recognized by the reticuloendothelial system (RES), which allows them to stay in circulation longer and, thus, enables larger accumulations of the drug at the target tumor site in order to minimize total systemic toxic effects, as compared to conventional therapy (e.g., chemotherapy). In fact, conventional anti-cancer drugs destroy healthy cells and injure healthy tissues, resulting in serious adverse effects on patients [3]. The use of nanomaterials for drug delivery is an area of concern for researchers and clinicians. The ability of nanomaterials used

* *Corresponding Author Email: mae.visit.04@uotechnology.edu.iq*

as drug carriers to enhance oral bioavailability and solubility, as well as to reduce the amount of drug necessary for administration, makes them attractive as a means of delivering chemotherapy agents to patients undergoing chemotherapy treatment. Another benefit of using nanomaterials for delivery of drug therapy is their ability to overcome drug resistance; therefore, the use of co-delivery systems that utilize nanocarriers may provide a feasible way to treat resistant cancers. Thus, it is feasible to use nanocarriers for drug delivery systems to carry the therapeutic agent, protect the therapeutic agent from physical and chemical degradation, provide selective targeting of ligands via functional groups, provide cellular access and facilitate release of the anti-cancer agent with improved therapeutic effectiveness.

Magnetic NPs can be degraded into Fe particularly in acidic cell compartments within the body such as lysosomes, which means that their long-term toxic effects are less likely to persist than are those for other inorganic NPs (e.g., carbon- and gold-based types) [6]. An additional feature of Fe oxide nanoparticles is that they can be created using a core shell model to prevent agglomeration in the form of clusters, allowing the gradual elimination of these NPs from the circulation [7]. Additionally, the surface coating of IONPs increases the permeability of drugs through the vascular system allowing for their easier transport across the endothelial barrier [8]. Furthermore, the modified surface can be functionalised with specific aptamers or antibodies to provide targeted delivery to specific cells. Finally, diversity in the targeted delivery of these NPs results from different types of functionalised surfaces, including peptides, antibodies and small molecules, which can all be easily attached to the surfaces of magnetic nanoparticles because of the intrinsic magnetic properties [9].

Iron oxide gives a unique property, thus being one of the most popular nanoparticles for medical application [10]. In particular, the use of Fe_2O_3 nanoparticles enhances both the stability and permeability of therapeutic agents as they pass through a tissue, and it increases the time the therapeutic agent will circulate within the body [11]. Therefore, using Fe_2O_3-based nano-carriers and delivering less total drug, benefits patients due to the ability to deliver the medicine in a more efficient manner and decrease the total amount of drug required to achieve effective therapy. Furthermore, the Fe_2O_3 nanoparticles are also capable of loading more than one drug molecule for controlled release of drugs in order to minimize toxicity or eliminate over-dosage by increasing the concentration of the medicine at locations within the body that do not contain healthy tissue [12]. Biocompatibility of the Fe_2O_3 NPs is one additional reason for the significant increase in interest that researchers have shown toward these NPs over the last several years. The properties of Fe_2O_3 NPs depend upon their surface morphology, crystalline structure, particle size and preparation method [13].

Additionally, magnetic nanoparticles exhibit electrocatalytic properties, allowing for fast readout of redox responsive delivery systems [14]. The controlled breakdown of a redox-responsive drug delivery system provides a fast release of encased drugs. Nano-carriers can be modified to employ enzyme-sensitive connections for on-demand, enzyme-sensitive drug delivery systems, decreasing the harmful effects of therapeutic agents. The effectiveness of these enzyme-sensitive nano-systems may allow for penetration into tumor tissue with unusual characteristics such as leaky vasculature and varied expression of enzymes. The use of the appropriate enzymes will also help in the development of Fe_2O_3 NPs with desirable characteristics. Since enzymes are endogenously sourced, they exhibit greater selectivity and catalysis in many biological processes compared to other substrates. Thus, they have been studied extensively as target substances in several endogenous and exogenous-stimuli sensitive systems [15]. In addition, the enzyme sensitivity of drug release increases both the speed at which drug is released from the nano-system into the tumor and the total quantity of drug that is concentrated in the tumor. In this way, redox responsive dual-stimuli responsive DDSs can significantly increase anti-cancer therapies through increasing drug accumulation, improving targeting of tumor cells and speeding drug release. Moreover, redox responsive delivery systems can be modified to include additional stimuli for better control of release rates and reduced side effects [16].

Nanoparticles have also been recently utilized in tissue engineering, as a means of simulating the extracellular matrix components of tissues to improve both mechanical and biological performance.

Furthermore, iron oxide nanoparticles have advantage of their shape and non toxicity, thus they can be used in a variety of ways on wounds. Wound dressings containing these nanoparticles can be used to promote physiological activity across the different phases of healing (acute/ chronic), thus promoting healing of the wound.

Fe_2O_3 has potential for functionalization and coating by appropriate polymers, to render these NPs as non-toxic, super magnetic, biocompatible and biodegradable; thus, positioning them as favorable materials for use in biomedical applications. Of these, burn injuries are perhaps the most serious and complex type of skin injury and pose considerable global medical burdens. The negative impact of burn injuries extends beyond just physical trauma, but also includes psychological and societal traumas; particularly in more severe cases of burns where patients are permanently disfigured or lose vital functions of the skin. In the year 2000, the World Health Organization (WHO) estimated that more than 3 million people globally suffer from burns every year with varying degrees of severity (due to thermal, chemical, electrical and radiated injuries). Specialized and timely medical care is often necessary in order to prevent significant complications, including infection, dehydration, and scarring [19].

Advancements in traditional treatments like topical creams, antibiotics, and dressings have proved largely ineffective with regards to extensive or deep burned skin injuries. Some patients experience slower wound healing, a higher likelihood of infections occurring, and the possibility of developing hypertrophic scarring or keloids. Innovative methods that will help optimize the human body's natural regenerative abilities and yield better clinical outcomes are urgently needed for this population [20].

In a recent study, nano-engineered scaffolds have been shown to speed up wound healing, as well as provide decreased rates of infection, stimulation of new blood vessel formation (angiogenesis), and enhanced skin restoration (both structurally and functionally), compared to traditional techniques. The clinical application of these new scaffolds has been found to be an extremely encouraging indication of their potential for use in treating patients with full thickness burns (which typically require grafting procedures). These findings have led to the objective of this study to investigate the effects of using nanomaterials and the tissue engineering of scaffolds for improved healing from burns. This investigation will also include an examination of the types of materials that make up the scaffolds and how they work, and how their incorporation into clinical practice might change the course of healing from burns in the future.

They serve as passive barriers against infection rather than means of promoting tissue regeneration or modulation of the inflammatory response. Complications during the healing of burns, such as infection, excessive inflammation, delayed epithelialization, and inadequate vascularity, may lead to prolonged hospital stays and higher risks for the development of hypertrophic scarring and death in some cases. [23] Table 1 Shows the clinical appearance of each degree of burn that may occur on the surface of the skin [24].

Different synthesis methods were used to create Fe_2O_3 and Fe_2O_3 -based materials of a variety of sizes and shapes (nanoparticles, nanotubes, nanorods, spindles, hollow nanostructures and porous nanostructures) via hydrothermal,

Table 1. Clinical characteristics according to the degree of depth.

Type of burn	Clinical appearance
First grade	Painful Pores the pressure Does not leave scar Heal 3-6 days
Second grade superficial	Pain, erythema, Flictenas Pale to pressure Heal in 7-20 days
Deep second grade	Include the reticular dermis Whitish, mottled, not paling under pressure Heal 2 to 5 weeks with large scar
Third grade	Hard, painless scalps Always require grafts

chemical precipitation, sol-gel, anodic oxidation and thermolysis techniques. Due to its ability to effectively control the size and shape as well as to minimize further 'agglomeration' of Fe_2O_3 nanoparticles, the hydrothermal method is generally preferred. Also, the use of the hydrothermal method leads to lower levels of impurity entering into the hydrolyzed product and is therefore more desirable compared to the other processes. In addition, hydrothermal processing requires relatively low reaction temperatures, is less expensive than other processes and is environmentally friendly. In addition to these advantages, Fe_2O_3 exists in two crystallographic

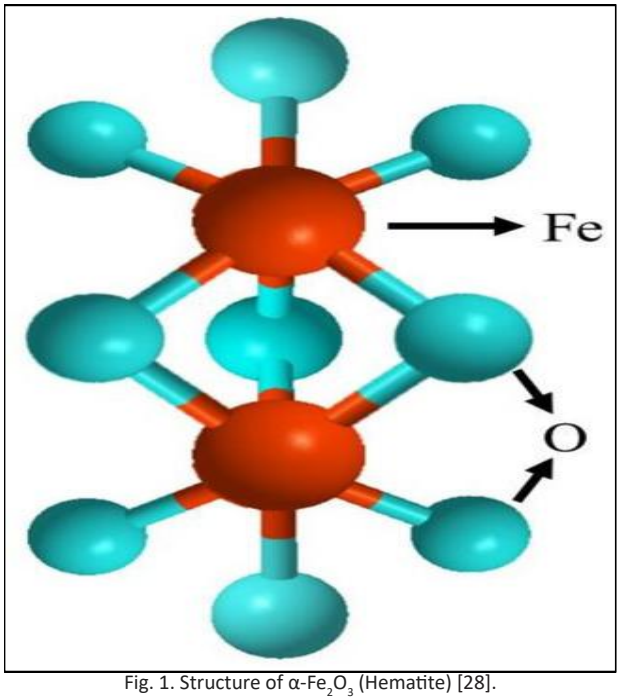

Fig. 1. Structure of α-Fe_2O_3 (Hematite) [28].

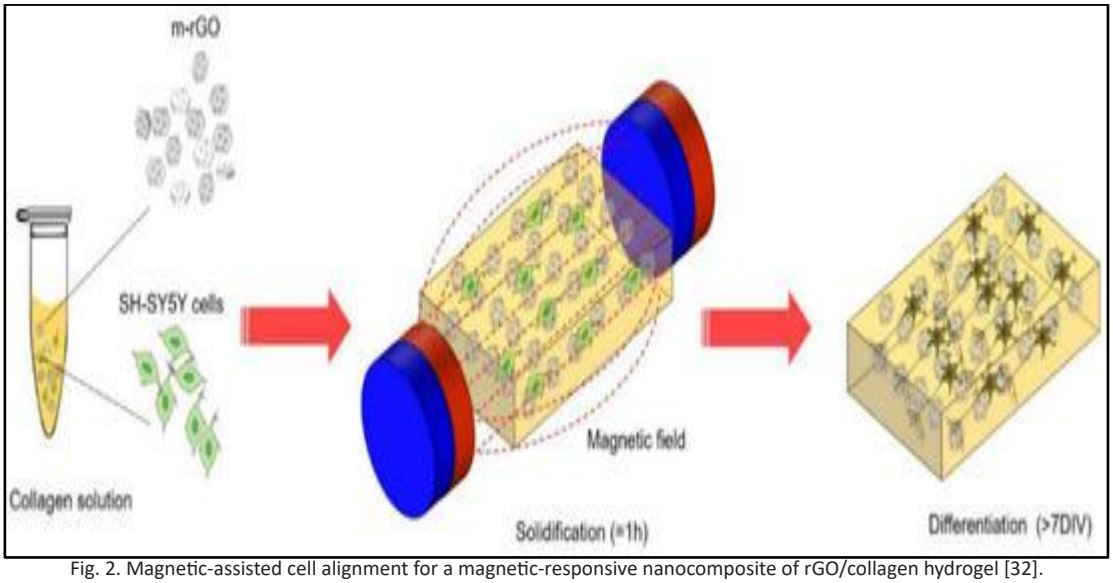

Fig. 2. Magnetic-assisted cell alignment for a magnetic-responsive nanocomposite of rGO/collagen hydrogel [32].

forms, α-Fe_2O_3 and γ-Fe_2O_3, as shown in Fig. 1. γ-Fe_2O_3 (maghemite) can be converted to α-Fe_2O_3 (Hematite) at high temperatures because α-Fe_2O_3 is the most thermodynamically stable phase of Fe_2O_3. The transition from α-Fe_2O_3 to γ-Fe_2O_3 requires either a nitrogen atmosphere with sufficient temperature control or the use of a reducing agent. In terms of changing from α-Fe_2O_3 to γ-Fe_2O_3, the morphology (shape or form) of the material is typically unchanged, which could allow for an effective means of producing controllable amounts of Fe_2O_3 with modified crystal structures. In terms of magnetic properties, due to their exchange bias and memory effects, α-Fe_2O_3 includes various magnetic phenomena. Additionally, small amounts of Fe_2O_3 (<10 nm) demonstrate superparamagnetic behavior and spin glass behavior [26]. The hexagonally shaped nanoparticles exhibit chemical reactivity, lack the ability to be cleaned by macrophages, exhibit long-term retention, conduct electricity and possess biocompatibility; therefore, they would be suitable materials for use in biomedical applications [27].

The primary purpose of tissue engineering is to use technology to create alternatives to natural tissues so that injured or damaged tissue can be maintained, restored, or improved in function [29]. Tissue engineering has sought to provide scaffolds that support both the structures and cells involved in the regeneration of tissues through mechanical support, and bioactive molecules to influence how cells will differentiate and function during the regeneration process [30]. Although there are many polymorphs of iron oxide, the most frequently researched forms of iron oxide in seeking to enhance tissue engineering applications are γ-Fe_2O_3 (maghemite), Fe_3O_4 (magnetite), and FeO (wustite). Of the three polymorphic forms of iron oxides, γ-Fe_2O_3 and Fe_3O_4 nanoparticles are the most commonly used in tissue engineering. These particular nanoparticles possess excellent properties for use in tissue engineering, including, but not limited to, being paramagnetic, having a high specific surface area, being biocompatible, and having low toxicity at the nanoscale level. Because of the desire of scientists and researchers to use biodegradable magnetic nanocomposites for biomedical applications because of the ability to create magnetic fields around objects, this is a growing area of research, particularly in relation to use in tissue regeneration and in the treatment of musculoskeletal disorders, such as osteoarthritis, which can be seen in Fig. 2 [31].

MATERIALS AND METHODS

The materials utilized in the experimental procedures included chemical substances biological models and laboratory equipment. A detailed list is presented below in Table 2

All materials were handled according to laboratory safety protocols. Solutions were prepared using sterile techniques to avoid contamination, especially when dealing with biological samples.

Preparation of Fe_2O_3NPs/PSL Nanocomposite

The preparation of the Fe_2O_3NPs/PSL nanocomposite involved a systematic multi-step process to ensure homogeneity and functional properties suitable for wound application.

Dissolution of Polystyrene Latex

Three grams of dried polystyrene latex (PSL) were accurately weighed using an analytical balance. The PSL powder was transferred into a clean 250 mL glass beaker. Subsequently, 50 mL of chloroform was added. The mixture was subjected to magnetic stirring at 500 rpm for 30 minutes at room temperature (approximately 25°C) to achieve complete dissolution. This step ensured

Table 2. The materials utilized in the experimental.

Material	Description	Quantity	Purpose
Polystyrene Latex (PSL)	Synthetic polymer $(C_8H_8)n$	3 grams	Carrier matrix
Fe2O3Nanoparticles	Metallic nanoparticles, size <100 nm	3 grams	Healing and antibacterial agent
Chloroform ($CHCl_3$)	Organic solvent, analytical grade	50 mL	Solvent for PSL
New Zealand White Rabbits	Healthy adult rabbits (2-2.5 kg)	6 rabbits	Animal model
Heating Rod	Metallic disc, adjustable temperature	-	Induction of controlled burns
Magnetic Stirrer	Laboratory-grade stirrer	-	Preparation of nanocomposite
Surgical Kit	Standard instruments	-	Burn induction and sampling
Histological Staining Kit	Hematoxylin and Eosin (H&E)	-	Tissue analysis
Digital Camera	High-resolution	-	Wound documentation
Analytical Balance	Precision ±0.001g	-	Material measurement

that the polymer chains were uniformly dispersed in the solvent, forming a clear viscous solution.

Incorporation of iron Nanoparticles

Three grams of iron nanoparticles were gradually added to the PSL solution under continuous stirring. The addition was performed slowly to prevent agglomeration of the nanoparticles. After complete addition, the mixture was stirred for an additional 1 hour to allow even distribution of Fe_2O_3 NPs within the PSL matrix.

Casting and Drying

The homogeneous Fe_2O_3NPs/PSL mixture was poured into sterile Petri dishes placed in a fume hood. The dishes were left undisturbed to allow the chloroform to evaporate slowly at room temperature over 24 hours. After complete solvent evaporation, thin flexible films of Fe_2O_3 NPs/PSL nanocomposite were obtained. These films were carefully peeled off and stored in sterile conditions until further use.

Experimental Animals

For the study, six adult healthy New Zealand White rabbits were acquired from a certified breeding facility and were acclimatized to the laboratory environment for 1 week before beginning the experiment. The rabbits were housed in individual cages made of stainless steel and in controlled conditions of temperature (22 ± 2° C) and humidity (relative humidity 50-60%), and light/dark cycle (12-hour cycles). During the experiment, rabbits were fed standard rabbit food and have free access to water throughout the experimental period. All procedures related to housing and care of the animals were performed according to the institution's ethical guidelines. The health of the rabbits was monitored on a daily basis, and all procedures were performed according to ethical guidelines for use of animals in research. The Institutional Animal Care and Use Committee approved the use of rabbits in this study. (IACUC).

Burn Induction Method

Controlled burns were induced on the dorsal surface of each rabbit under aseptic conditions. Local anesthesia (lidocaine 2%) was administered to minimize pain and distress. As explain in Table 3.

Burn Induction Steps

The back of each rabbit was carefully shaved and disinfected with 70% ethanol before the burns were inflicted. A metal disc, preheated to 100°C, was then applied vertically to the skin with light, controlled pressure to induce thermal burns. Each rabbit received two burn wounds, one first-degree and one second-degree, in two adjacent but separate dorsal areas. After the burns were inflicted, the affected areas were left uncovered for 10 minutes before the application of the appropriate treatment formulations.

Treatment Protocol

Following burn induction Treatment Group: Application of Fe_2O_3NPs/PSL nanocomposite

Table 3. Burn Induction Method.

Burn Type	Temperature	Exposure Time	Location
First-Degree	100°C	10 seconds	Upper dorsal area
Second-Degree	100°C	20 seconds	Lower dorsal area

Table 4. Clinical Evaluation of Healing.

Day	Parameters Assessed	Observation
0	Initial wound size, redness, blistering	Severe in second-degree burns
7	Scab formation, reduction in redness, wound contraction	More advanced in treated group
14	Re-epithelialization, disappearance of scab, skin texture	Complete in first-degree treated wounds

film, cut to the size of the wound, secured with sterile bandages. And Control Group Covered with standard sterile gauze dressing without active treatment. The dressing was changed every two days. The wound sites were cleaned gently using saline solution during dressing changes to prevent secondary infection. for clinical evaluation of healing the wound healing was evaluated based on multiple parameters as seen in Table 4.

Histological Analysis

To further evaluate the effectiveness of the Fe_2O_3NPs/PSL nanocomposite in promoting wound healing, histological examination was conducted after 14 days. Tissue biopsies were collected from the wound areas under general anesthesia and immediately fixed in 10% neutral buffered formalin for 24 hours.

Tissue Processing

The collected tissue samples underwent a series of preparation steps for histological examination. Initially, the tissues were dehydrated using a graduated series of ethanol solutions (70%, 80%, 90%, 95%, and 100%), then cleaned in xylene to remove residual alcohol. Next, the dehydrated samples were immersed in paraffin wax molds, and thin sections approximately 5 µm thick were prepared using a microtome. Finally, the tissue sections were placed on clean glass slides and allowed to dry before staining and microscopic analysis.

Staining Protocol (Hematoxylin and Eosin)

For histological staining, tissue sections were immersed in hematoxylin for 5 minutes to highlight cell nuclei, then rinsed with tap water in a blue staining step to enhance nuclear staining intensity. Next, the sections were stained with eosin for 1 minute to highlight cytoplasmic and extracellular structures. The stained sections were then gradually dried using graded ethanol solutions, cleaned with xylene, and finally mounted using DPX fixation medium and covered with glass slides before microscopic examination.

Comparative Tables of Healing

The healing outcomes were compared between treated and untreated groups for both first- and second-degree burns. Clinical Comparison in Table 5.

Biological Mechanism of Skin Healing

Following a burn injury, the skin healing process consists of three overlapping biological phases. The Inflammatory Phase (Days 0-3) includes the following two biological responses: First is the vascular response, where blood vessels increase in size (dilate) and allow protein and cells to move out of circulation and into the tissue; and second, the cellular response, in which immune cells, primarily neutrophils and macrophages, are mobilized to invade the affected, damaged tissue and begin the process of tissue repair and protect against infection. The addition of the ferric oxide/polystyrene nanoparticle to the burn area will also help protect the damaged skin and reduce the risk of developing an infection during the inflammatory phase because of its antibacterial properties. The Proliferative Phase

Table 5. Clinical Comparison.

Day	Parameter	First-Degree Control	First-Degree Treated	Second-Degree Control	Second-Degree Treated
0	Redness	+++	+++	++++	++++
7	Scab Formation	++	+++	++	+++
14	Wound Contraction	65%	90%	40%	70%
14	Re-epithelialization	Partial	Complete	Partial	Moderate

(+: mild, ++: moderate, +++: strong, ++++: very strong)

Table 6. Histological Comparison.

Parameter	First-Degree Control	First-Degree Treated	Second-Degree Control	Second-Degree Treated
Re-epithelialization	Partial	Complete	Absent	Partial
Granulation Tissue	Thin	Moderate	Moderate	Thick
Angiogenesis	Moderate	Abundant	Sparse	Moderate
Inflammatory Infiltration	Mild	Very mild	Severe	Moderate
Necrosis	None	None	Present	Mild

(Days 4-10) includes the key biological process of wound healing through fibroblast activation, angiogenesis, and epithelial remodeling. Fibroblasts become activated as they migrate to and proliferate in the wound (granulation) and produce and deposit the extracellular matrix into the wound area. Continued and simultaneous to fibroblast activation is the process of angiogenesis, which provides new capillaries that supply oxygen and critical nutrients to the newly formed tissue. Epithelial remodeling can also be seen as a result of keratinocytes migrating across the wound surface to restore epidermal continuity and promote healing of the wound. The Remodeling Phase of Wound Healing (Day 11 Onward). Significant tissue reorganization will occur during this tissue remodeling phase of the wound healing process. There is a progressive replacement of type III collagen with type I collagen with this process. The end result of; type I collagen produced contributes to the overall strength (i.e., tensile strength) and overall integrity (i.e., structural integrity) of the regenerating tissue. As the metabolic needs of the tissue heal, capillary regression occurs and the excess blood vessels created via angiogenesis, will also decrease. Through the tissue maturation process, the function and strength of the skin are restored to its original function and mechanical properties, approaching that of normal uninjured skin. The Fe_2O_3 NPs/PSL nanocomposite enhanced all phases of wound healing with an apparent acceleration of angiogenesis while exhibiting a decrease in extended inflammation.

Statistical Analysis Methodology

Although the sample size was limited, descriptive statistics were applied as Wound area measurements were recorded and presented as mean ± standard deviation. A comparative assessment of the experimental groups was performed based on the percentage of wound shrinkage observed on day 14 post-treatment. Additionally, a qualitative histological assessment was conducted to evaluate tissue regeneration parameters, including the inflammatory response, fibroblast proliferation, angiogenesis, and epithelial remodeling.

RESULTS AND DISCUSSION

Ray Diffraction for Iron Fe_2O_3\PLS components

The synthesized nanomaterial of iron (Fe_2O_3) and PLS based on plant materials shows an amorphous structure when viewed under the XRD (X-Ray Diffraction Pattern). The mild crystalline structure was detected by using the Debye-Scherrer formula (Fig. 4). An explanation

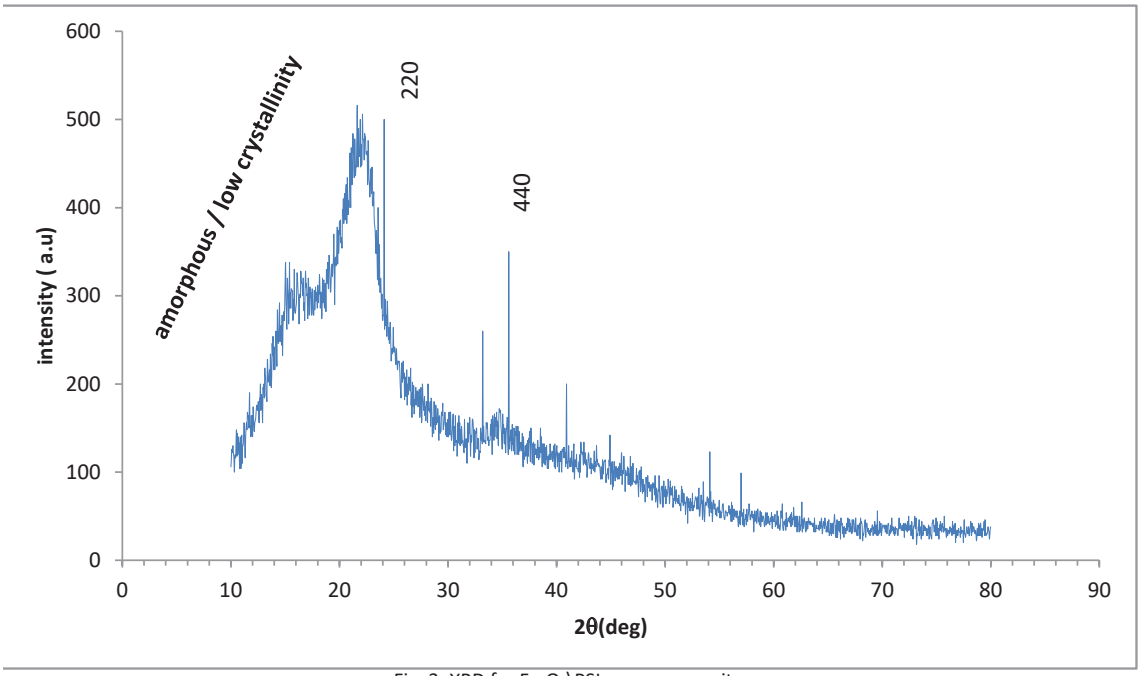

Fig. 3. XRD for Fe_2O_3\PSL nanocomposite.

of this is that the synthesis of this material in the presence of polymers and organic materials without an inorganic phase is affecting the long-range structure of the material by controlling the amount of crystalline structure that forms and preventing any from forming through the action of the organic molecules from the plant material coating and stabilising the material being synthesised create difficulties in the formation of long-range order and would lead to the absence of any visible diffraction peaks [33]. This generally is seen as due to the ultra-fine crystal structure or strongly embedded within the amorphous region thus inhibiting the formation of crystalline structure has occurred due to the inhibiting action of the coating and stabilising effect of the plant molecules during the synthesis of the material thus inhibiting crystal growth and aggregation of the inorganic phase [34]. The amorphous nature of this material helps to improve wound healing through increased elasticity, swelling capacity, and moisture retention, thereby providing an ideal microenvironment for tissue regeneration. Similar amorphous or low crystallinity has also been found to exist in a variety of environmentally friendly nanocomposites and bio-composites, where structural disorder is associated with enhanced biological performance [35].

Scanning Electron Microscopes (SEM) for Fe_2O_3\ PSL nanocomposite

Polystyrene latex polymer combined with ferric oxide composite's Scanning Electron Microscope (SEM) image depicts the existence of a heterogeneous surface made up of spherical particles within a polymer matrix and clustered Fe_2O_3 fluffy crystals, indicating there was an excellent interaction or bonding of both the inorganic and polymer phase will be visually apparent in Fig. 4 as there are varying degrees of distribution on a single image of nano-sized particles with surface flaking and agglomeration due to adhesion between particles during the preparation process. Porosity (air voids) and coarse surfaces are indicative of increased, effective surface area of the composite material [36-37].

The Fourier transform infrared (FTIR) for Fe_2O_3\PSL Nano-Composite

The Fourier Transform Infrared (FTIR)

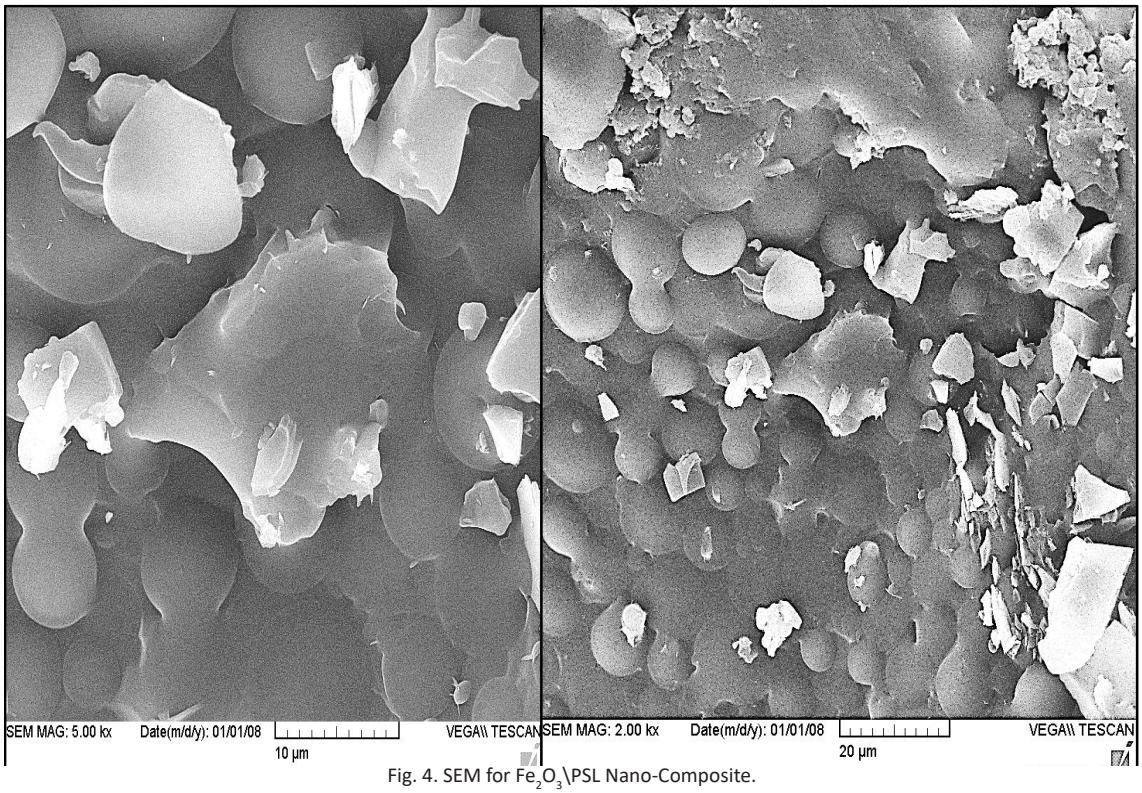

Fig. 4. SEM for Fe_2O_3\PSL Nano-Composite.

Spectroscopy was conducted on the synthesized Nanocomposite to confirm successful Polymerization (PDS) in the Surface Polymer Layer (PSL) and to yield a Chemical Reactive Hybrid system. The broad band around 3250 cm^{-1} is due to stretching of O-H bonds from Hydroxyl (OH) groups in both the Polymer matrix and phytochemiacl components, and the presence of moisture adsorbed. This peak also shows potential formation of hydrogen bonds between the polymer chains contributing to the structural stability of the composite. The weak band around 2925 cm^{-1} reflects aliphatic C-H stretching of the core polymer structure. The band near 1600 cm^{-1} arises from aromatic C=C stretching of phenolic compounds or from H-O-H bending of water molecules indicating that bioactive chemicals were incorporated into the matrix/component (Fig. 5). The intense spectral bands observed between 1000 and 1100 cm^{-1} are due to stretching vibrations of the C–O bonds from alcohols, phenols, and ether functional groups, which agree with those shown in Fig. 1 and confirm a chemical contribution of these groups to the polymer network structure. Overall, these spectral characteristics show that the polymer acts not just as a physical vehicle but contributes to intermolecular interactions and forms a cohesive organic matrix. The presence of these interactions is necessary for successful use of the polymer as a wound dressing, as those interactions improve the stability of the membrane, the retention of moisture in the membrane and allow for controlled release of bioactive substances [39].

Clinical Evaluation of Wound Healing

Following the induction of first- and second-degree burns on the dorsal surfaces of rabbits, the

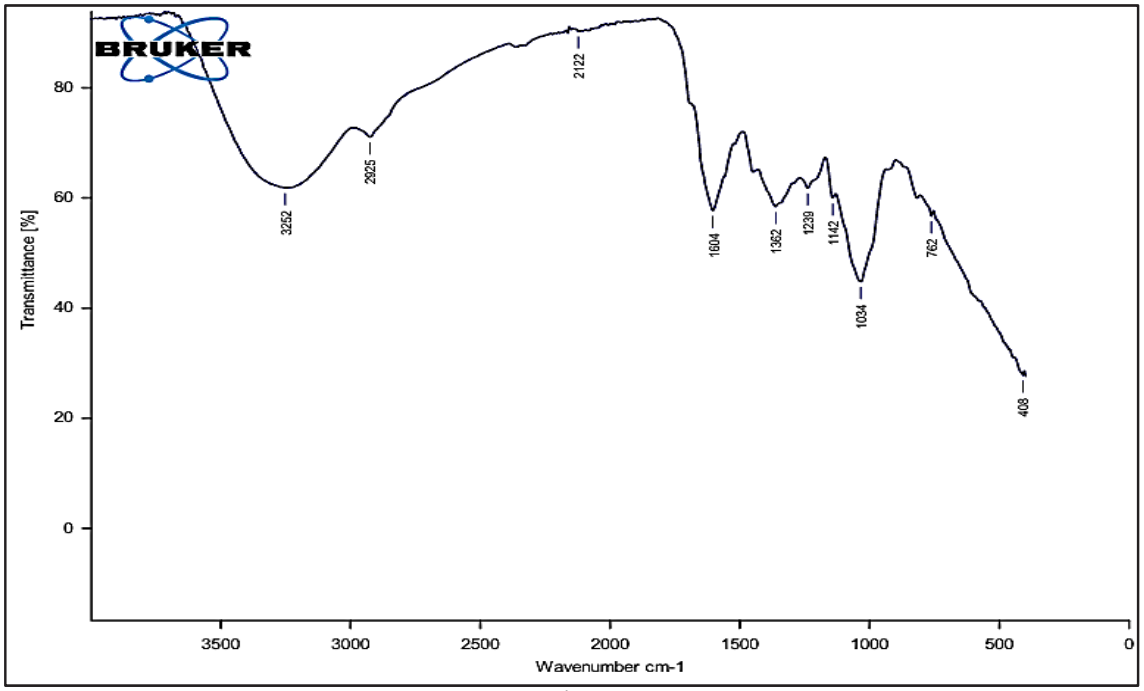

Fig. 5. FR-IR for Fe_2O_3\PSL Nano-Composite.

Table 7. The overall wound contraction percentages are summarized below.

Group	Wound Type	Wound Contraction at Day 14 (%)
Treated	First-Degree	92%
Treated	Second-Degree	75%
Control	First-Degree	68%
Control	Second-Degree	48%

Fe_2O_3/PSL nanocomposite dressing was applied to the experimental wounds, while control wounds were treated with conventional sterile gauze. The healing process was monitored over a 14-day period through visual observation, wound diameter measurements, and clinical scoring.

First-Degree Burns

In the Fe_2O_3NPs/PSL-treated wounds, scab formation was observed by day 3, followed by significant wound contraction by day 7 and complete re-epithelialization by day 13, with near-normal skin texture and minimal discoloration, whereas the control wounds exhibited slower contraction, persistent redness, and only partial re-epithelialization by day 14.

Second-Degree Burns

The treated second-degree burns exhibited early granulation tissue formation by day 7, with significant reduction in wound size by day 14. However, complete re-epithelialization was not fully achieved in second-degree treated burns within the 14-day observation period. Control second-degree burns showed extensive necrotic tissue, persistent inflammation, and delayed

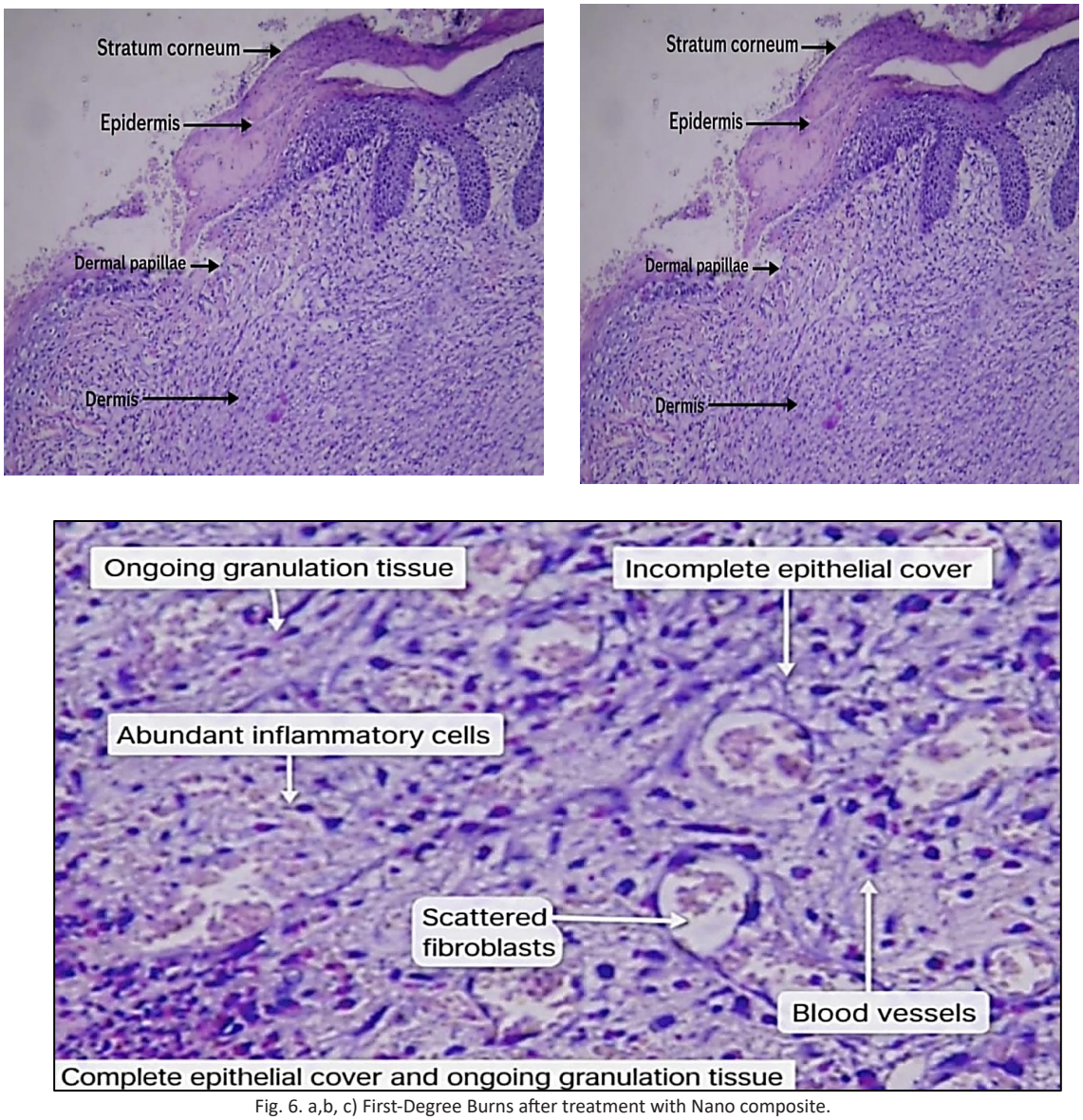

Fig. 6. a,b, c) First-Degree Burns after treatment with Nano composite.

healing compared to treated wounds [40].

Histological Evaluation

Histological analysis provided deeper insight into the quality of tissue regeneration. For the first-degree burns and as seen in Fig. 6a, of presence of a protective scab and early granulation tissue formation under the scab. And in Fig. 6b Initiation of stratified epithelial layer regeneration; active fibroblast proliferation observed. In Fig. 6c, Mature granulation tissue with abundant new capillary formation, minimal inflammatory cell infiltration,

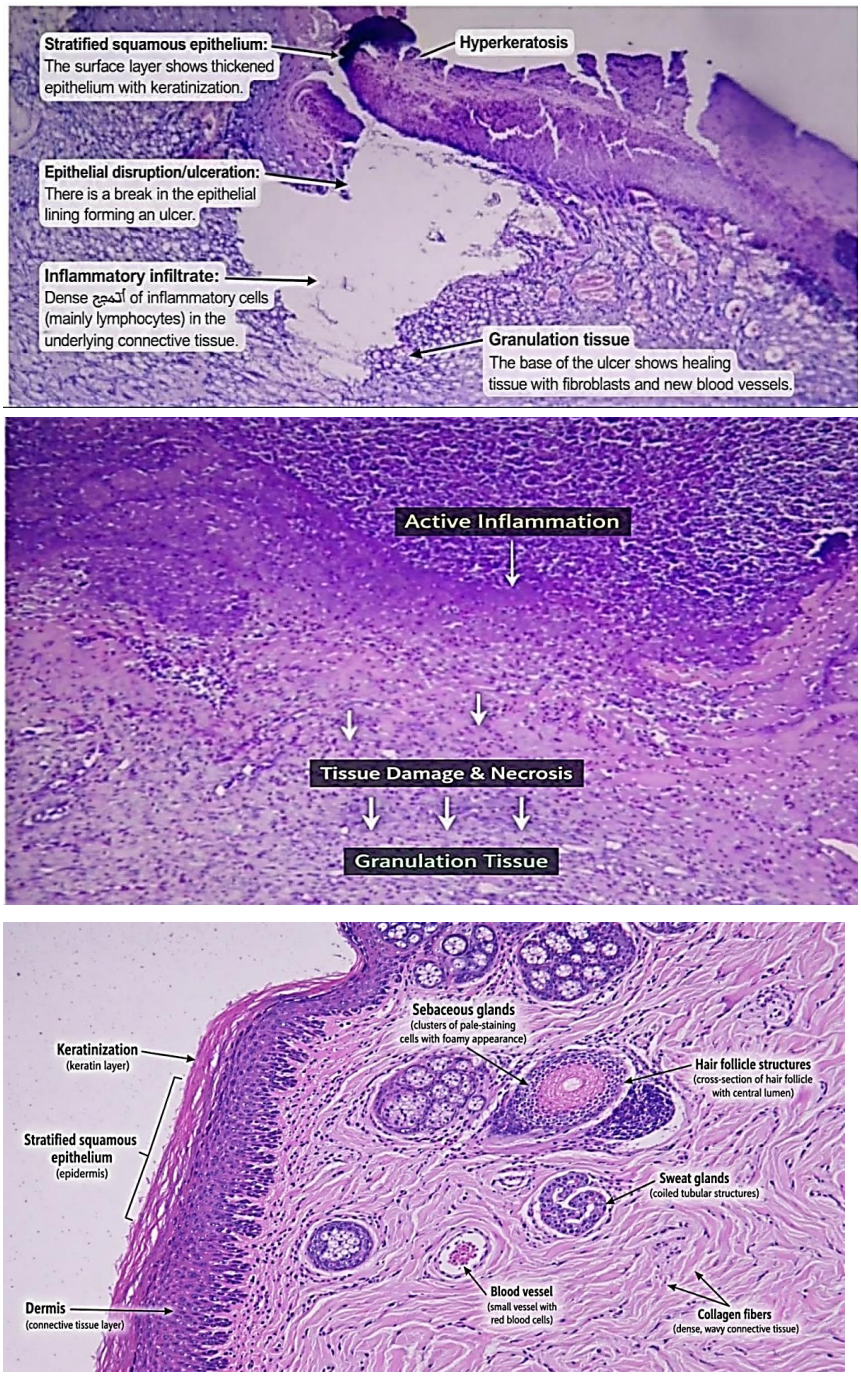

Fig. 7. a,b, c) Second-Degree Burns after treatment with Nano composite.

Table 8. Comparative Analysis Fe_2O_3 /PSL-treated wounds and controls.

Parameter	Treated (Fe_2O_3 /PSL)	Control
Wound Closure Rate	Faster	Slower
Scab Detachment Time	Earlier (10–11 days)	Delayed (13–15 days)
New Epithelium Thickness	Thicker, organized	Thinner, disorganized
Inflammatory Cell Infiltration	Mild to moderate	Severe
Vascularization	Abundant	Sparse
Presence of Necrosis	Minimal (second-degree only)	Extensive

and progressing collagen deposition [41].

For the Second-Degree Burns and at seen in Figs.7a, b and c. Severe epidermal and partial dermal damage; incomplete epithelial cover and ongoing granulation tissue formation. Fig. 7b seen formation of an abscess surrounded by dense inflammatory infiltrates, indicating secondary infection risk and at Fig. 7c it is noticed Necrotic tissue presence, extensive inflammatory infiltration, delayed epithelial regeneration [42].

In contrast to the control wounds, Fe_2O_3Ps/ PSL-treated wounds had well-organized dermal structures, significantly greater capillary development, and less inflammatory infiltration than the untreated control wounded animals. Fe_2O_3 has been shown to reduce inflammation, thereby reducing the time period for recovery from inflammation and allowing for the accelerated transition through the proliferative and remodeling phases of healing. Therefore, as a result of the different degrees of tissue damage and cellular destruction associated with first- and second-degree burns, the healing time required to recover from an injury of this type is longer in patients with second-degree burns, as compared to patients with first-degree burns, even when using new and improved technology. Finally, because of the relatively uncomplicated and inexpensive process of fabricating Fe_2O_3 /PSL films, these types of materials provide an opportunity for large-scale production and application within clinical settings. Further evidence for this ability has been reported elsewhere.

The rapid recovery documented in the wounds treated with Fe_2O_3 NPs/PSL is due to a combination of factors. These include: Strong Antibacterial Effects of Fe_2O_3 NP, resulting in a reduction of local bacterial counts, thus also reducing the potential for infection during critical early stages of healing. Promotion of Angiogenesis due to the stimulation of endothelial cell proliferation and increased VEGF levels by Fe_2O_3 results in increased levels of neovascularization necessary for the delivery of oxygen and other nutrients. Lastly, enhanced fibroblasts within the PSL scaffold create an ideal environment for fibroblasts to attach and migrate; this aids in the formation of the ECM [46-47].

Comparative Analysis

The following key in Table 8 differences were observed between Fe_2O_3/PSL-treated wounds and controls.

CONCLUSION

The purpose of the study was to investigate the ability of a dressing made of a Fe 2 O3/ PSL nanocomposite to heal first- and second-degree burns using a rabbit model. The primary conclusion of the study shows that the healing process was accelerated in rabbits with first-degree burns treated with a Fe_2O_3/PSL dressing; the rate of wound contraction, scab detachment, and complete re-epithelialization was significantly greater than for control groups. Clinical evaluations and histological analyses showed mature and well-organized layers of skin were created with minimal evidence of inflammatory infiltrates. Second Degree Burn Patients Have Better Healing Dynamics. Despite being slowed down by depth (due to being on deeper tissues), patients that received treatment had a more organized granulation tissue (wounds), early growth of new blood vessels (early neoviable), and less necrosis (death of tissue) than those that did not receive treatment (untreated controls). There was histological evidence of tissue regeneration in treated second-degree burn patients. Based on microscopic examination, there was significant evidence of new fiber cell production, high amounts of vascular cells and early fibrous tissue matrix accumulation in the experimental group (comparatively) that suggest improved tissue re-modelling phases when compared with no treatment. No evidence of a secondary infection occurred within any of the wound sites in the experimental groups, indicating that the use of

Fe_2O_3 provided adequate anti-microbial protection during the whole period of tissue repair. There are probably other biological mechanisms of action associated with a nanocomposite dressing to enhance wound healing by stimulating the formation of new blood vessels, diminishing the occurrence of persistently inflamed wounds, and permitting operative cellular movement/ multiplication. The nanocomposite (Fe_2O_3/PSL) dressing was able to produce physiologically quicker and/or better paced wound healing than standard treatments used on first degree burns; as well as, show at least as good as if not greater amounts of healed tissue on second degree burn sites when using the nanocomposite dressing than when using standard treatment methods.

CONFLICT OF INTEREST

The authors declare that there is no conflict of interests regarding the publication of this manuscript.

REFERENCES

1. Iqbal MZ, Wu A. Magnetic Nanohybrids for Magnetic Resonance Imaging and Phototherapy Applications. Frontiers in Nanobiomedical Research: World Scientific; 2017. p. 101-149. http://dx.doi.org/10.1142/9789813149199_0005
2. Pourmadadi M, Ahmadi M, Abdouss M, Yazdian F, Rashedi H, Navaei-Nigjeh M, et al. The synthesis and characterization of double nanoemulsion for targeted Co-Delivery of 5-fluorouracil and curcumin using pH-sensitive agarose/chitosan nanocarrier. J Drug Deliv Sci Technol. 2022;70:102849.
3. Brero F, Albino M, Antoccia A, Arosio P, Avolio M, Berardinelli F, et al. Hadron Therapy, Magnetic Nanoparticles and Hyperthermia: A Promising Combined Tool for Pancreatic Cancer Treatment. Nanomaterials. 2020;10(10):1919.
4. Ferreira LP, Reis CP, Robalo TT, Melo Jorge ME, Ferreira P, Gonçalves J, et al. Assisted Synthesis of Coated Iron Oxide Nanoparticles for Magnetic Hyperthermia. Nanomaterials. 2022;12(11):1870.
5. Staudinger U, Janke A, Simon F, Jakisch L, Bittrich E, Formanek P, et al. MWCNT Localization and Electrical Percolation in Thin Films of Semifluorinated PMMA Block Copolymers. Polymers. 2025;17(9):1271.
6. Samadi A, Haseli S, Pourmadadi M, Rashedi H, Yazdian F, Navaei-Nigjeh M. Curcumin-loaded Chitosan-Agarose-Montmorillonite Hydrogel Nanocomposite for the Treatment of Breast Cancer. 2020 27th National and 5th International Iranian Conference on Biomedical Engineering (ICBME); 2020/11/26: IEEE; 2020. p. 148-153.
7. Mirzaie Z, Barati M, Tokmedash MA. Anticancer Drug Delivery Systems Based on Curcumin Nanostructures: A Review. Pharm Chem J. 2020;54(4):353-360.
8. Tokmedash MA, Seyyedi Zadeh E, Balouchi EN, Salehi Z, Ardestani MS. Synthesis of smart carriers based on tryptophan-functionalized magnetic nanoparticles and its application in 5-fluorouracil delivery. Biomedical Materials. 2022;17(4):045026.
9. Fusser M, Øverbye A, Pandya AD, Mørch Ý, Borgos SE, Kildal W, et al. Cabazitaxel-loaded Poly(2-ethylbutyl cyanoacrylate) nanoparticles improve treatment efficacy in a patient derived breast cancer xenograft. Journal of Controlled Release. 2019;293:183-192.
10. Samadi A, Pourmadadi M, Yazdian F, Rashedi H, Navaei-Nigjeh M, Eufrasio-da-silva T. Ameliorating quercetin constraints in cancer therapy with pH-responsive agarose-polyvinylpyrrolidone -hydroxyapatite nanocomposite encapsulated in double nanoemulsion. Int J Biol Macromol. 2021;182:11-25.
11. Gao X, Wang B, Wei X, Men K, Zheng F, Zhou Y, et al. Anticancer effect and mechanism of polymer micelle-encapsulated quercetin on ovarian cancer. Nanoscale. 2012;4(22):7021.
12. Shabnam H, Mehrab P, Amirmasoud S, Fatemeh Y, Majid A, Hamid R, et al. Author response for "A novel-responsive nanoniosomal emulsion for sustained release of curcumin from a chitosan-based nanocarrier: emphasis on the concurrent improvement of loading, sustained release, and apoptosis induction". Wiley; 2022. http://dx.doi.org/10.1002/btpr.3280/v2/response1
13. Jasim AJ, Yusop MR, Taha BA, Al-Amiery AA, Saadoon NM, Akhtar MF, et al. Sustainable development of novel zinc oxide nano flowers mediated red yeast rice for control of hepatocellular carcinoma. Sci Rep. 2026;16(1).
14. Rahmani E, Pourmadadi M, Ghorbanian SA, Yazdian F, Rashedi H, Navaee M. RETRACTED: Preparation of a pH-responsive chitosan-montmorillonite-nitrogen-doped carbon quantum dots nanocarrier for attenuating doxorubicin limitations in cancer therapy. Eng Life Sci. 2022;22(10):634-649.
15. Lee ALZ, Wang Y, Cheng HY, Pervaiz S, Yang YY. The co-delivery of paclitaxel and Herceptin using cationic micellar nanoparticles. Biomaterials. 2009;30(5):919-927.
16. Sun C, Lee JSH, Zhang M. Magnetic nanoparticles in MR imaging and drug delivery. Adv Drug Del Rev. 2008;60(11):1252-1265.
17. Mohammed MQ, Shugran AHM. Inhibitory effect of silver oxide nanoparticles and Saccharomyces cerevisiae on Escherichia coli and Staphylococcus aureus bacteria. Experimental and Theoretical NANOTECHNOLOGY. 2026;10(1):13-23.
18. Yu MK, Park J, Jon S. Targeting Strategies for Multifunctional Nanoparticles in Cancer Imaging and Therapy. Theranostics. 2012;2(1):3-44.
19. Kanwar JR, Roy K, Kanwar RK. Chimeric aptamers in cancer cell-targeted drug delivery. Critical Reviews in Biochemistry and Molecular Biology. 2011;46(6):459-477.
20. Rahdar S, Rahdar A, Ahmadi S, Trant JF. Adsorption of bovine serum albumin (BSA) by bare magnetite nanoparticles with surface oxidative impurities that prevent aggregation. Can J Chem. 2019;97(8):577-583.
21. Davarpanah AM, Rahdar A, Dastnae MA, Zeybek O, Beyzaei H. (1-x)$BaFe_{12}O_{19}$/ x$CoFe_2O_4$ hard/soft magnetic nanocomposites: Synthesis, physical characterization, and antibacterial activities study. J Mol Struct. 2019;1175:445-449.
22. Taimoory SM, Rahdar A, Aliahmad M, Sadeghfar F, Hajinezhad MR, Jahantigh M, et al. Corrigendum to "The synthesis and characterization of a magnetite nanoparticle with potent antibacterial activity and low mammalian

toxicity" [J. Mol. Liq. 265 (2018) 96–104]. J Mol Liq. 2019;277:989.
23. Nouri Hajbaba M, Pourmadadi M, Yazdian F, Rashedi H, Abdouss M, Zhohrabi DS. The function of chitosan/agarose biopolymer on Fe_2O_3 nanoparticles and evaluation of their effects on MCF-7 breast cancer cell line and expression of BCL2 and BAX genes. Biotechnology Progress. 2022;39(1).
24. Saadoon AM, Al Gharawi M, Al-Mosawe A. Effect of Elevated Temperature on Microstructure and Mechanical Properties of Hot-Rolled Steel. Engineering, Technology and Applied Science Research. 2024;14(6):18756-18766.
25. Qiao Z, Shi X. Dendrimer-based molecular imaging contrast agents. Prog Polym Sci. 2015;44:1-27.
26. Rahdar A, Taboada P, Aliahmad M, Hajinezhad MR, Sadeghfar F. Iron oxide nanoparticles: Synthesis, physical characterization, and intraperitoneal biochemical studies in Rattus norvegicus. J Mol Struct. 2018;1173:240-245.
27. Ahmadi M, Pourmadadi M, Ghorbanian SA, Yazdian F, Rashedi H. Ultra pH-sensitive nanocarrier based on Fe_2O_3/chitosan/montmorillonite for quercetin delivery. Int J Biol Macromol. 2021;191:738-745.
28. Mishra M, Chun D-M. α-Fe_2O_3as a photocatalytic material: A review. Applied Catalysis A: General. 2015;498:126-141.
29. Debnath NC, Anderson AB. Optical Spectra of Ferrous and Ferric Oxides and the Passive Film: A Molecular Orbital Study. J Electrochem Soc. 1982;129(10):2169-2174.
30. Abdalsalam A, Saadoon N, Ati A, Dabagh S, Salim A. Investigation of the structural, morphological, and electrochemical characteristics of $MgFe_2O_4$/ZnO nanocomposite. Al-Qadisiyah Journal for Engineering Sciences. 2025;18(4):352-359.
31. Ye Y, Chen H, Zou Y, Ye Y, Zhao H. Corrosion protective mechanism of smart graphene-based self-healing coating on carbon steel. Corros Sci. 2020;174:108825.
32. Hmoad NR, Ali AH, Saadoon AM, Abdulkareem AA, Albayati AH. Effect of different wing geometries on their vibration characteristics. Frontiers in Mechanical Engineering. 2026;11.
33. Shahriari M, Zahiri M, Abnous K, Taghdisi SM, Ramezani M, Alibolandi M. Enzyme responsive drug delivery systems in cancer treatment. Journal of Controlled Release. 2019;308:172-189.
34. Li R, Peng F, Cai J, Yang D, Zhang P. Redox dual-stimuli responsive drug delivery systems for improving tumor-targeting ability and reducing adverse side effects. Asian Journal of Pharmaceutical Sciences. 2020;15(3):311-325.
35. Gharawi MA, Saadoon AM, Hmoad NR, Albayati AH. Structural performance of rail connections: Experimental testing and finite element modeling. Results in Engineering. 2025;27:105997.
36. Xu Y, Xiao L, Chang Y, Cao Y, Chen C, Wang D. pH and Redox Dual-Responsive MSN-S-S-CS as a Drug Delivery System in Cancer Therapy. Materials. 2020;13(6):1279.
37. Rahmah MI, Saadoon NM, Mohasen AJ, Kamel RI, Fayad TA, Ibrahim NM. Double hydrothermal synthesis of iron oxide/silver oxide nanocomposites with antibacterial activity **. Journal of the Mechanical Behavior of Materials. 2021;30(1):207-212.
38. Abdullah NH, Shameli K, Abdullah EC, Abdullah LC. Solid matrices for fabrication of magnetic iron oxide nanocomposites: Synthesis, properties, and application for the adsorption of heavy metal ions and dyes. Composites Part B: Engineering. 2019;162:538-568.
39. Eivazzadeh-Keihan R, Bahojb Noruzi E, Khanmohammadi Chenab K, Jafari A, Radinekiyan F, Hashemi SM, et al. Metal-based nanoparticles for bone tissue engineering. J Tissue Eng Regen Med. 2020;14(12):1687-1714.
40. Kim K, Fisher JP. Nanoparticle technology in bone tissue engineering. Journal of Drug Targeting. 2007;15(4):241-252.
41. Zhang S, Vijayavenkataraman S, Lu WF, Fuh JYH. A review on the use of computational methods to characterize, design, and optimize tissue engineering scaffolds, with a potential in 3D printing fabrication. Journal of Biomedical Materials Research Part B: Applied Biomaterials. 2018;107(5):1329-1351.
42. Eltom A, Zhong G, Muhammad A. Scaffold Techniques and Designs in Tissue Engineering Functions and Purposes: A Review. Advances in Materials Science and Engineering. 2019;2019:1-13.
43. Rajendran NK, Kumar SSD, Houreld NN, Abrahamse H. A review on nanoparticle based treatment for wound healing. J Drug Deliv Sci Technol. 2018;44:421-430.
44. Chai M, Tong W, Wang Z, Chen Z, An Y, Zhang Y. Piezoelectric-Fenton degradation and mechanism study of Fe_2O_3/PVDF-HFP porous film drove by flowing water. J Hazard Mater. 2022;430:128446.
45. Harandi FN, Khorasani AC, Shojaosadati SA, Hashemi-Najafabadi S. Surface modification of electrospun wound dressing material by Fe_2O_3 nanoparticles incorporating Lactobacillus strains for enhanced antimicrobial and antibiofilm activity. Surfaces and Interfaces. 2022;28:101592.
46. Shahali M, Khandan A, Raisi A, Asefnejad A, Sadat Kazerouni Z, Kolooshani A, et al. Preparation, characterization, and antibacterial studies of N, O-carboxymethyl chitosan as a wound dressing for bedsore application. Archives of Trauma Research. 2020;9(4):181.
47. Tadic M, Kopanja L, Panjan M, Lazovic J, Tadic BV, Stanojevic B, et al. Rhombohedron and plate-like hematite (α-Fe_2O_3) nanoparticles: synthesis, structure, morphology, magnetic properties and potential biomedical applications for MRI. Mater Res Bull. 2021;133:111055.